Interplay of quantum magnetic and potential scattering around Zn or Ni impurity ions in superconducting cuprates

Guang-Ming Zhang[1], Hui Hu[2], Lu Yu[2,3]

[1] *Center for Advanced Study, Tsinghua University, Beijing 100084, China*

[2] *Abdus Salam International Center for Theoretical Physics, P. O. Box 586, Trieste 34100, Italy*

[3] *Institute of Theoretical Physics and Interdisciplinary Center of Theoretical Studies, Academic Sinica, Beijing 100080, China*

(February 1, 2008)

Abstract

To describe the scattering of superconducting quasiparticles from non-magnetic (Zn) or magnetic (Ni) impurities in optimally doped high T_c cuprates, we propose an effective Anderson model Hamiltonian of a localized electron hybridizing with $d_{x^2-y^2}$-wave BCS type superconducting quasiparticles with an attractive scalar potential at the impurity site. Due to the strong local antiferromagnetic couplings between the original Cu ions and their nearest neighbors, the localized electron in the Ni-doped materials is assumed to be on the impurity sites, while in the Zn-doped materials the localized electron is distributed over the four nearest neighbor sites of the impurities with a dominant $d_{x^2-y^2}$ symmetric form of the wave function. Since both scatterings from the localized electron and the scalar potential are relevant, localized resonant states due to their interplay are formed below the maximal superconducting gap. With Ni impurities, two resonant states are formed above the Fermi level in the local density of states at the impurity site, while for Zn impurities a sharp resonant peak below the Fermi level dominates in the local density of states at the Zn site, accompanied by a small and broad reso-

nant state above the Fermi level mainly induced by the potential scattering. This is exactly what has been observed in the scanning tunneling microscopy experiments. In both cases, there are no Kondo screening effects. From the calculated spin relaxation functions, we find that the 3d localized electron in both Ni and Zn doped materials displays a weak magnetic oscillation. This result is consistent with the signal of a spin-1/2 magnetic moment exhibited by nuclear magnetic resonance measurements in $YBa_2Cu_3O_{6+\delta}$ doped with Zn or Ni impurities. The local density of states and their spatial distribution at the dominant resonant energy around the substituted impurities are calculated for both cases, and they are in good agreement with the experimental results of scanning tunneling microscopy in $Bi_2Sr_2CaCu_2O_{8+\delta}$ with Zn or Ni impurities, respectively. Thus the scanning tunneling and nuclear magnetic resonance experiments on Zn and Ni substituted cuprates are interpreted self-consistently in a unified fashion.
PACS numbers: 71.10.Hf, 71.27.+a, 71.55.-i, 75.20.Hr

I. INTRODUCTION

Recent experiments on d-wave superconducting cuprates have shown many interesting phenomena in the presence of magnetic (Ni) and non-magnetic (Zn) impurities substituting the Cu ions in the copper-oxygen plane. A series of nuclear magnetic resonance (NMR) experiments on optimally doped $YBa_2Cu_3O_{6+\delta}$ with impurities [1–3] have shown that each non-magnetic impurity (Zn) induces a local spin-1/2 magnetic moment on the neighboring Cu sites, while a magnetic (Ni) impurity gives rise to a localized spin-1/2 magnetic moment on the impurity site. On the other hand, scanning tunneling microscopy (STM) has been used to probe the quasiparticle scattering around single Zn or Ni impurity ions in optimally doped $Bi_2Sr_2CaCu_2O_{8+\delta}$ with high spatial and energy resolution [4,5]. In the obtained STM spectra, a very sharp localized resonance peak is found just below the zero-bias voltage on the Zn impurity sites [4], while two localized resonant states are formed well above the zero-bias voltage on the Ni impurity sites [5]. The spatial dependence of the local density of states (LDOS) in the vicinity of the individual impurity ions reveals the characteristic features of $d_{x^2-y^2}$ wave superconducting (dSC) states, but the pattern is different in these two cases.

A large number of theoretical papers have been devoted to the interpretation of these beautiful experimental data. According to one school of thoughts, this is due to a potential scattering, either spin-independent, or magnetic (classical magnetic moment) [6–10]. In fact, the quasi-bound state around a potential scatter in d-wave superconductors was discussed before the experiments were done [6,8]. On the other hand, there is an alternative explanation ascribing the resonant scattering as due to the Kondo effect in d-wave superconductors [11–13], extending earlier studies of the Kondo effect in systems with reduced density of states at the Fermi level [14,15]. It is fair, however, to say that several important issues remain unexplained, for example, the strong particle-hole asymmetry, the difference between the Zn- and Ni-doped cases, concerning both spectral distribution and spatial pattern. Thus a full understanding of these experiments is still lacking.

In an earlier communication [16], we proposed an effective Anderson Hamiltonian with hybridization of a localized electron with quasiparticles in d-wave superconducting states to describe the scattering on quantum magnetic impurities. In the limit of the Hubbard repulsion $U \to \infty$, we have shown the existence of a sharp resonance above the Fermi level and absence of the Kondo screening. Moreover, a "marginal Fermi liquid" behavior was found for the impurity electron self-energy in the strong coupling limit. In this paper we extend our study to include the potential scattering effect on the impurity site. The interplay of the quantum magnetic scattering and potential scattering turns out to play a very important role in determining the spectral distribution and spatial pattern.

The NMR [1–3] and neutron scattering [17] experiments show that Zn doping has a stronger disturbance to the antiferromagnetic background in cuprates than Ni doping. There is a kind of common understanding that Zn doping induces a local magnetic moment distributed mostly over the nearest neighbor Cu ions, whereas Ni impurity has an underscreened $S = 1/2$ moment, sitting on the Ni ion itself. This picture is consistent with the electron configurations. Zn^{2+} ions have a closed shell ($3d^{10}$, $S = 0$), with an extra d-electron compared with Cu^{2+} which is not entirely sitting on the Zn site. The electronic structure studies [18] do show that the electron charge density is higher on neighboring oxygen sites and nearest neighbor Cu^{2+} ions. On the other hand, Ni^{2+} ions ($3d^8$, $S = 1$) have an extra hole of spin 1/2 on site, compared with Cu^{2+} ions, and the deficit of charge is concentrated on the Ni site. [18] In this paper, we propose a unified model to describe these two cases. We consider a local charge carrier ($3d$ electron in the Zn case and $3d$ hole in the Ni case, to be called Anderson electrons for short, and such a treatment is allowed due to the particle-hole symmetry of the BCS state) with a strong on-site Coulomb repulsion U, is hybridizing with superconducting quasiparticles of $d_{x^2-y^2}$ symmetry. In the Ni-doped case, the Anderson electron is sitting on the impurity site itself, whereas in the Zn-doped case, it is distributed over the nearest neighbor Cu^{2+} ions. The dominant contribution comes from the linear combination with $d_{x^2-y^2}$ symmetry. Moreover, we assume an attractive δ-type potential scattering in both cases, which can be justified to some extent within the three-band Hubbard model . [19]

In the above effective model, due to a strong interplay between the quantum impurity scattering (described by the Anderson model) and the potential scattering of the quasiparticles in dSC state, we find a sharp resonance state below the Fermi energy mainly due to the Anderson electron, and a broad potential scattering peak in the positive energy in the LDOS for the Zn-doped case. In contrast, two resonance peaks due to Anderson electron and potential scattering are formed well above the Fermi level for the Ni-doped case. These distinct features fully agree with STM experiments [4,5]. Moreover, the spatial pattern of the resonance states differs in these two cases, also in agreement with experiments. The calculated dynamical spin response functions show typical structures corresponding to the existence of local magnetic moments. These results demonstrate convincingly that the proposed unified model describes the essential physics of these experiments self-consistently.

The rest of the paper is organized as follows. In section II, the nickel impurity substitution is considered, with both Anderson electron and potential scattering center located at the impurity site itself. In section III, we discuss the interplay of quantum magnetic scattering on the Anderson electron distributed over nearest neighbors and on-site potential scattering, corresponding to the Zn-doped case. Finally, concluding remarks are made in section IV.

II. MODEL CALCULATION FOR NICKEL IMPURITY SUBSTITUTION

To construct a simple model, we assume that a BCS-type weak coupling theory is applicable as a phenomenological framework for high-T_c optimally doped superconductors, though the underlying mechanisms are very different. When the Cu ions on the CuO_2 plane are replaced by magnetic Ni impurities, there will be one extra 3d hole on each impurity ion. Due to the particle-hole symmetry of the dSC quasiparticles, we can work in the electron representation, and assume that the magnetic Ni impurity is effectively described by the Anderson localized electron with a strong Hubbard repulsion. Moreover, a scalar *attractive* potential at the impurity site has been added to the model Hamiltonian as caused by interactions with the nearest neighbor Cu ions. When the correlations between the magnetic

impurities on different sites are ignored, the model Hamiltonian is defined as

$$\begin{aligned}\mathcal{H} = & \sum_{\mathbf{k}\sigma} \epsilon_{\mathbf{k}} c^{+}_{\mathbf{k}\sigma} c_{\mathbf{k}\sigma} + \sum_{\mathbf{k}} \Delta_{\mathbf{k}} \left(c^{+}_{\mathbf{k}\uparrow} c^{+}_{-\mathbf{k}\downarrow} + h.c. \right) \\ & + \frac{W}{N} \sum_{\mathbf{k},\mathbf{k}',\sigma} c^{+}_{\mathbf{k}\sigma} c_{\mathbf{k}'\sigma} + \epsilon_d \sum_{\sigma} d^{+}_{\sigma} d_{\sigma} \\ & + \frac{V}{\sqrt{N}} \sum_{\mathbf{k}\sigma} \left(c^{+}_{\mathbf{k}\sigma} d_{\sigma} + h.c. \right) + U d^{+}_{\uparrow} d_{\uparrow} d^{+}_{\downarrow} d_{\downarrow}, \end{aligned} \tag{1}$$

where $\epsilon_{\mathbf{k}} = \hbar^2 k^2/(2m) - \epsilon_F$ is the dispersion of the normal state electrons, $\Delta_{\mathbf{k}} = \Delta_0 \cos 2\theta$ is the dSC order parameter with the gap amplitude Δ_0, and $W < 0$ is the strength of the attractive potential. When Nambu spinors are introduced

$$\hat{\psi}_{\mathbf{k}} = \begin{pmatrix} c_{\mathbf{k}\uparrow} \\ c^{+}_{-\mathbf{k}\downarrow} \end{pmatrix}, \qquad \hat{\varphi} = \begin{pmatrix} d_{\uparrow} \\ d^{+}_{\downarrow} \end{pmatrix},$$

we rewrite the model Hamiltonian in a matrix from

$$\begin{aligned}\mathcal{H} = & \sum_{\mathbf{k}} \hat{\psi}^{+}_{\mathbf{k}} \left(\epsilon_{\mathbf{k}} \sigma_z + \Delta_{\mathbf{k}} \sigma_x \right) \hat{\psi}_{\mathbf{k}} + \frac{W}{N} \sum_{\mathbf{k},\mathbf{k}'} \hat{\psi}^{+}_{\mathbf{k}} \sigma_z \hat{\psi}_{\mathbf{k}'} \\ & + \frac{V}{\sqrt{N}} \sum_{\mathbf{k}} \left(\hat{\psi}^{+}_{\mathbf{k}} \sigma_z \hat{\varphi} + h.c. \right) \\ & + (\epsilon_d + \frac{U}{2})(\hat{\varphi}^{+} \sigma_z \hat{\varphi} + 1) - \frac{U}{2} (\hat{\varphi}^{+} \hat{\varphi} - 1)^2, \end{aligned} \tag{2}$$

where σ_z and σ_x are Pauli matrices. The equations of motion for the dSC quasiparticles yield the generalized $\mathbf{T}$-matrix *exactly*

$$\begin{aligned}\hat{T}(i\omega_n) = & V^2 [\sigma_z - W \hat{G}_0(i\omega_n)]^{-1} \hat{G}_d (i\omega_n) [\sigma_z - W \hat{G}_0(i\omega_n)]^{-1} \\ & + W [\sigma_z - W \hat{G}_0(i\omega_n)]^{-1}, \end{aligned} \tag{3}$$

where $\hat{G}_0(i\omega_n) = \frac{1}{N} \sum_{\mathbf{k}} (i\omega_n - \epsilon_{\mathbf{k}} \sigma_z - \Delta_{\mathbf{k}} \sigma_x)^{-1}$ is the GF of the dSC quasiparticles at the impurity site. When the scalar potential is absent, the T-matrix is reduced to

$$\hat{T}(i\omega_n) = V^2 \sigma_z \hat{G}_d (i\omega_n) \sigma_z, \tag{4}$$

which was obtained previously in the single impurity Anderson model in dSC electron state [16]. On the other hand, if only the scalar potential is present, it becomes

$$\hat{T}\left(i\omega_n\right) = [(W\sigma_z)^{-1} - \hat{G}_0(i\omega_n)]^{-1}, \tag{5}$$

which is the same result as derived by Balatsky *et al.* [6]. From the generalized T-matrix, one can clearly see that *both hybridization with the localized electron and potential scattering are equally important in determining the low energy excitations.* At zero temperature, analytical continuation is used to calculate the perturbed GF through the following relation:

$$\hat{G}\left(\mathbf{r},\mathbf{r}';\omega\right) = \hat{G}^0\left(\mathbf{r}-\mathbf{r}',\omega\right) + \hat{G}^0\left(\mathbf{r},\omega\right)\hat{T}\left(\omega\right)\hat{G}^0\left(-\mathbf{r}',\omega\right).$$

The LDOS of the dSC quasiparticles around the impurity is given by

$$N\left(\mathbf{r},\omega\right) = -\frac{1}{\pi}\,\mathrm{Im}\,\hat{G}_{11}\left(\mathbf{r},\mathbf{r};\omega\right).$$

We would emphasize that the above relation between the GF of the dSC quasiparticles and the Anderson electron is *exact*, and the only quantity to determine is $\hat{G}_d(\omega)$, which will be calculated approximately.

When we take the infinite U limit, the localized electron operator is expressed as $\widehat{\varphi}^+ = \left(f_\uparrow^+ b,\ f_\downarrow b^+ \right)$ in the slave-boson representation [20,21], where the fermion f_σ and the boson b describe the singly occupied and hole states, respectively. The constraint $b^+b + \sum_\sigma f_\sigma^+ f_\sigma = 1$ has to be imposed. When a mean field approximation is applied, the boson operators b and b^+ are replaced by a c-number b_0, and the constraint is treated by introducing a chemical potential λ_0. Therefore, the mean field Hamiltonian is written as

$$\begin{aligned}\mathcal{H}_{mf} = &\sum_{\mathbf{k}} \hat{\psi}_{\mathbf{k}}^+ \left(\epsilon_{\mathbf{k}}\sigma_z + \Delta_{\mathbf{k}}\sigma_x\right)\hat{\psi}_{\mathbf{k}} + \frac{W}{N}\sum_{\mathbf{k},\mathbf{k}'} \hat{\psi}_{\mathbf{k}}^+ \sigma_z \hat{\psi}_{\mathbf{k}'} \\ &+ \frac{\tilde{V}}{\sqrt{N}}\sum_{\mathbf{k}} \left(\hat{\psi}_{\mathbf{k}}^+ \sigma_z \widehat{\phi} + h.c.\right) + \tilde{\epsilon}_d \widehat{\phi}^+ \sigma_z \widehat{\phi} \\ &+ \tilde{\epsilon}_d + \lambda_0(b_0^2 - 1).\end{aligned} \tag{6}$$

where $\widehat{\phi}^+ = \left(f_\uparrow^+,\ f_\downarrow \right)$denotes the Nambu spinors of the localized electron and the renormalized parameters $\tilde{\epsilon}_d = \epsilon_d + \lambda_0$ and $\tilde{V} = b_0 V$. It has been known that the slave-boson mean field approximation produces the correct low energy physics of the conventional Anderson impurity model in the entire parameter range at zero temperature, though strong quantum

fluctuations are present near the Fermi surface from the gapless excitations of the conduction electrons [22]. In the present model, we are dealing with dSC quasiparticles, where a superconducting gap exists on most part of the Fermi surface except four nodal points, we thus expect that the slave-boson mean field approximation should work better than the conventional case, giving rise to more reliable results at zero temperature.

The standard techniques lead to $\hat{G}_f(i\omega_n) = \left[i\omega_n - \tilde{\epsilon}_d\sigma_z - \hat{\Sigma}_f\left(i\omega_n\right)\right]^{-1}$, where the self-energy of the localized electron becomes,

$$\hat{\Sigma}_f\left(i\omega_n\right) = \tilde{V}^2[\hat{G}_0^{-1}(i\omega_n) - W\sigma_z]^{-1}. \tag{7}$$

At $T = 0$, the ground-state energy changes due to the presence of localized electron and the scalar potential are:

$$\begin{aligned}\delta\varepsilon = -\frac{1}{\pi}\int_0^D d\omega \ln\left[\omega^2\left(1+b_0^2\beta\right)^2 + \left[\tilde{\epsilon}_d - b_0^2(W/V^2)\omega^2\alpha\beta\right]^2\right] \\ +\tilde{\epsilon}_d + \lambda_0\left(b_0^2 - 1\right),\end{aligned}$$

where D is the band width of the normal conduction electrons, $\alpha(\omega) = \frac{1}{N}\sum_{\mathbf{k}}\frac{V^2}{\omega^2+\epsilon_{\mathbf{k}}^2+\Delta_{\mathbf{k}}^2}$, and $\beta(\omega) = \frac{\alpha(\omega)}{1+(W/V^2)\omega^2\alpha^2(\omega)}$. The corresponding saddle-point equations are derived as

$$\lambda_0 = \frac{1}{\pi}\int_0^D d\omega \frac{2\omega^2\beta(1+b_0^2\beta) - 2(W/V^2)\omega^2\alpha\beta\left[\tilde{\epsilon}_d - b_0^2(W/V^2)\omega^2\alpha\beta\right]}{\omega^2\left(1+b_0^2\beta\right)^2 + \left[\tilde{\epsilon}_d - b_0^2(W/V^2)\omega^2\alpha\beta\right]^2}, \tag{8}$$

$$b_0^2 = \frac{1}{\pi}\int_0^D d\omega \frac{2\left[\tilde{\epsilon}_d - b_0^2(W/V^2)\omega^2\alpha\beta\right]}{\omega^2\left(1+b_0^2\beta\right)^2 + \left[\tilde{\epsilon}_d - b_0^2(W/V^2)\omega^2\alpha\beta\right]^2}. \tag{9}$$

For given parameters D, Δ_0, $\Gamma = \pi N_F V^2$, ϵ_d, and $c = \pi N_F|W|$, one can obtain saddle point values of b_0 and λ_0. In the following calculations, we choose Δ_0 as the energy unit, $D/\Delta_0 = 20$, and $\Gamma/\Delta_0 = 0.2$.

The phase diagram can be obtained for a specific value of the potential scattering strength c, similar to the phase diagram given previously [16]. When ϵ_d is less than a threshold value, b_0^2 is zero, leading to a free local magnetic moment decoupled from the dSC quasiparticles. Above the threshold value of ϵ_d, b_0^2 rises sharply and then saturates. The low energy behavior of the model is controlled by the nearly empty orbital state, characterized by a

strong hybridization between the Anderson electron and the dSC quasiparticles. In the hole representation, the empty orbital phase corresponds to a single hole occupation at the Ni impurity site. Such a situation can not be realized in the conventional Anderson impurity model, where the low energy behavior is always controlled by the Kondo screening fixed point in the single electron occupied phase. The dSC quasiparticles actually provide us with such a possibility to explore new low-energy physics in the empty orbital regime — the strong coupling behavior in the single hole occupied regime. In a sense, such a strong coupling behavior is also universal, corresponding to a new strong coupling fixed point without any characteristic energy scale. However, the scalar potential will introduce some extra features to the LDOS around the impurities.

We have seen that both scalar potential and localized electron scatterings are relevant in the dSC state, and two resonant states are formed with a dominant sharp localized resonance *above* the Fermi level. In Fig. 1, we plot the DOS for the localized electron $N_d(\omega)$ with different values of ϵ_d for two potential scattering strengths $c = 1$ and 2. For a small ϵ_d, the resonant peak positions can be roughly determined as

$$\Omega^1_{res} \approx \tilde{\epsilon}_d \left[1 - b_0^2 \left(\frac{2\Gamma}{\pi\Delta_0}\right) \ln \frac{4\Delta_0}{\tilde{\epsilon}_d}\right],\ \Omega^2_{res} \simeq \Delta_0 \frac{\pi}{2c \ln(8c/\pi)}. \tag{10}$$

Clearly, the former resonance peak is mainly induced by the localized Anderson electron, while the latter weaker resonance is caused by the attractive potential. As ϵ_d moves up, the magnitude of the first localized resonance Ω^1_{res} decreases and becomes broader with shifting upward of the peak position, while the magnitude of the second resonance Ω^2_{res} emerges as a pronounced peak at a relative high energy. When $\epsilon_d \sim 0.30$, the profile of the two consecutive resonances agrees well with the measured DOS at individual Ni site [5]. This does also confirm our assumption of the *attractive* scalar potential at the Ni impurity site, because the corresponding localized resonant state would appear below the Fermi energy if the scalar potential scattering is repulsive.

The nature of the double resonant peaks in the DOS of localized electrons can also be understood from the imaginary part of its retarded self-energy:

$$\mathrm{Im}\,\Sigma_{f,}^{1,1}\left(\omega+i0^{+}\right)=\mathrm{Im}\,\frac{b_0^2\Gamma}{(\pi N_F)G_0^{-1}(\omega+i0^{+})+c}, \tag{11}$$

which has been plotted in Fig.2a. In contrast to the case in the absence of attractive scalar potential (solid line), a single peak appears above the Fermi energy (dashed line), corresponding to the pole of Eq. (11). This peak becomes narrower with increasing the potential strength c (dash-dotted line). Moreover, the existence of the scalar potential greatly suppresses the spectrum weight of the self-energy far away from the Fermi level. However, the marginal Fermi liquid behavior [23] obtained previously is preserved: $\mathrm{Im}\,\Sigma_{f,}^{1,1}(\omega)\sim -b_0^2\Gamma\left(\frac{|\omega|}{\Delta_0}\right)$as $\omega\to 0$.

Furthermore, in order to reveal the characteristic behavior in the regime of the empty orbital (single hole) localized state, we calculate the dynamic spin response function of the localized electron

$$\chi_d(t,t')=\langle\langle S_d^z(t):S_d^z(t')\rangle\rangle \tag{12}$$

corresponding to particle-hole collective excitations, from which the spin relaxation function $S_d(\omega)=-\frac{1}{\pi}\frac{\chi_d''(\omega+i0^{+})}{\omega}$ can be evaluated. $S_d(\omega)$ is related to the neutron scattering cross-section and the calculated value is displayed in Fig.2b. There is a pair of symmetric peaks demonstrating *a weak magnetic oscillation* for the $3d$ localized hole, in contrast to the universal result of one central resonant peak obtained in the Kondo regime of the conventional Anderson impurity model [24]. Such a behavior is consistent with a local spin 1/2 magnetic moment on the Ni impurity site observed in the NMR measurements [3]. We also notice that closer the localized resonant state is to the Fermi level, stronger magnetic oscillation the localized hole exhibits. This can be understood by considering the linear energy dependence of the LDOS for the dSC quasiparticles: the localized resonant state becomes more and more delocalized as one moves away from the Fermi level. As for the self-energy, the presence of potential scattering ($c\neq 0$) reduces substantially the magnitude of the spin relaxation function.

Now consider the LDOS of the dSC quasiparticles $N(\mathbf{r},\omega)$ in the spatial range $0<\mathbf{r}\leq\xi$. In high T_c dSC state, ξ is about 10Å, or roughly 3 lattice spacings. In Fig. 3, the LDOS vs

frequency is shown for r=0.07ξ from the impurity site along the vertical (or horizontal) and diagonal directions in real space. Similar to the LDOS for the localized electron, there are two resonances above the Fermi energy along the diagonal (the gap nodal) directions and the LDOS is entirely hole-like. In contrast, for vertical and horizontal (the gap maximum) directions, two more resonant peaks appear below the Fermi level as well, which are slightly asymmetric in the line shape and strongly reminiscent of the localized bound states induced by paramagnetic impurities in the conventional s-wave superconducting state [25]. In both of these cases, increasing the potential strength will sharpen and enhance the localized resonances significantly. As the impurity energy level ϵ_d moves up, the quasiparticle resonances become broader, exhibiting a similar dependence as the resonance of the Anderson electron itself.

It is very important to calculate the spatial distribution of the LDOS of dSC quasiparticles to compare with corresponding STM results. The LDOS around the impurity at the first resonance energy is displayed in Fig.4a for the hole-like excitations $\omega = -\Omega^1_{res}$ and in Fig.4b for the electron-like excitations $\omega = \Omega^1_{res}$ as a function of spatial variables for $c = 1, 2,$ and 3 with $\epsilon_d/\Delta_0 = -0.05$ in a logarithmic intensity scale. The quasiparticle resonances induced by substituted impurities are highly localized around the impurity, and the spatial oscillation of these resonant states is visible. The largest amplitude of the quasiparticle resonance occurs in the neighborhood of the impurity, and the local electronic structures distinctly differ in Fig.4a from that in Fig.4b. For $\omega = \Omega^1_{res}$, the LDOS exhibits a four-fold symmetry along the directions of the gap nodes for all distances, consistent with the dSC quasiparticles. For $\omega = -\Omega^1_{res}$, the LDOS is strongly enhanced in the gap maxima directions at distances $r \ll \xi$. Further away from the impurity ($r\sim\xi$), it is confined to the neighborhood of the diagonal directions, preserving the four-fold symmetry. At the same time, the LDOS of the dSC quasiparticles at the impurity site (the center of the diagram) and around the impurity site get enhanced by increasing the strength of the scalar potential. In fact, these features have been seen in the STM experiment [5], namely, the resonance at positive energy is enhanced in the nodal directions, while the resonance at negative energy

is more visible in the anti-nodal directions. To the best of our knowledge, these distinctive features have not been explained by other theoretical models considered so far. The absence of particle-hole symmetry is natural in our consideration, due to the quantum origin of the resonant states, and it is in full agreement with STM experiments. [5]

III. MODEL CALCULATION FOR ZINC IMPURITY SUBSTITUTION

In the high T_c cuprates, the substitution of Cu ions by Zn impurities adds an additional $3d$ electron to each Cu ion. By carefully analyzing the experimental results [1,2,4], one can notice that local antiferromagnetic correlations around the non-magnetic impurities get enhanced. As a result, there should be a localized magnetic moment distributed mainly over the four nearest neighbors of Zn impurities with an *attractive* scalar potential at the impurity. In the following, we will work in the electron representation, and assume that the localized state is still described by the Anderson localized electron with a strong on-site Hubbard repulsion. The effective model Hamiltonian is thus given by:

$$\begin{aligned}\mathcal{H} = & \sum_{\mathbf{k}\sigma} \epsilon_{\mathbf{k}} c^{+}_{\mathbf{k}\sigma} c_{\mathbf{k}\sigma} + \sum_{\mathbf{k}} \Delta_{\mathbf{k}} \left(c^{+}_{\mathbf{k}\uparrow} c^{+}_{-\mathbf{k}\downarrow} + h.c. \right) \\ & + \frac{W}{N} \sum_{\mathbf{k},\mathbf{k}',\sigma} c^{+}_{\mathbf{k}\sigma} c_{\mathbf{k}'\sigma} + \epsilon_d \sum_{\sigma} d^{+}_{\sigma} d_{\sigma} \\ & + \frac{1}{\sqrt{N}} \sum_{\mathbf{k}\sigma} V_{\mathbf{k}} \left(c^{+}_{\mathbf{k}\sigma} d_{\sigma} + h.c. \right) + U d^{+}_{\uparrow} d_{\uparrow} d^{+}_{\downarrow} d_{\downarrow}. \end{aligned} \tag{13}$$

Compared with the previous model Hamiltonian for the nickel substitution, the momentum dependence of the hybridization strength takes the form of $V_{\mathbf{k}} = V \cos 2\theta$, because the Anderson electron sitting on the four nearest neighbor sites of the Zn impurity hybridizes with the dSC quasiparticles with a dominant $d_{x^2-y^2}$ symmetric form of the wave function. This is the most effective coupling channel in the dSC [11,13]. The model Hamiltonian now describes an *extended* Anderson quantum "impurity" coupled with the dSC quasiparticles. In terms of the Nambu spinors, the GF of the conduction electrons is deduced from the equations of motion

$$\hat{G}(\mathbf{k},\mathbf{k}';i\omega_n) = \delta_{\mathbf{k},\mathbf{k}'}\hat{G}_0(\mathbf{k},i\omega_n) + \frac{1}{N}\hat{G}_0(\mathbf{k},i\omega_n)\hat{T}_{\mathbf{k},\mathbf{k}'}(i\omega_n)\hat{G}_0(\mathbf{k}',i\omega_n), \tag{14}$$

where the generalized **T**-matrix becomes momentum dependent. After Fourier transformation, the above equation is expressed explicitly as

$$\begin{aligned}
&\hat{G}\left(\mathbf{r},\mathbf{r}';i\omega_n\right) \\
&= \hat{G}^0\left(\mathbf{r}-\mathbf{r}',i\omega_n\right) + \hat{G}^0\left(\mathbf{r},i\omega_n\right)\hat{T}_0\left(i\omega_n\right)\hat{G}^0\left(-\mathbf{r}',i\omega_n\right) \\
&+V^2\hat{G}_i^0\left(\mathbf{r},i\omega_n\right)\sigma_z\hat{G}_d\left(i\omega_n\right)\sigma_z\hat{G}_i^0\left(-\mathbf{r}',i\omega_n\right) \\
&+V^2\hat{G}_i^0\left(\mathbf{r},i\omega_n\right)\sigma_z\hat{G}_d\left(i\omega_n\right)\sigma_z\hat{G}^0\left(\mathbf{r}_0,i\omega_n\right)\hat{G}_p^0\left(i\omega_n\right)\hat{G}^0\left(-\mathbf{r}',i\omega_n\right) \\
&+V^2\hat{G}^0\left(\mathbf{r},i\omega_n\right)\hat{G}_p^0\left(i\omega_n\right)\hat{G}^0\left(\mathbf{r}_0,i\omega_n\right)\sigma_z\hat{G}_d\left(i\omega_n\right)\sigma_z\hat{G}_i^0\left(-\mathbf{r}',i\omega_n\right),
\end{aligned} \tag{15}$$

with a momentum independent part of the T-matrix

$$\hat{T}_0\left(i\omega_n\right) = \hat{G}_p^0\left(i\omega_n\right) + V^2\hat{G}_p^0\left(i\omega_n\right)\hat{G}^0\left(\mathbf{r}_0,i\omega_n\right)\sigma_z\hat{G}_d\left(i\omega_n\right)\sigma_z\hat{G}^0\left(\mathbf{r}_0,i\omega_n\right)\hat{G}_p^0\left(i\omega_n\right),$$

where $\hat{G}_p^0\left(i\omega_n\right) = W[\sigma_z - W\hat{G}_0(i\omega_n)]^{-1}$ is the resulting GF for the dSC quasiparticles at the impurity site in the presence of the potential scattering only, $\hat{G}^0\left(\mathbf{r}_0,i\omega_n\right) = \frac{1}{NV}\sum_{\mathbf{k}} V_{\mathbf{k}}\hat{G}_0(\mathbf{k},i\omega_n)$ corresponds to the GF at the localized electron site, and $\hat{G}_i^0\left(\mathbf{r},i\omega_n\right) = \frac{1}{NV}\sum_{\mathbf{k}} V_{\mathbf{k}}\hat{G}_0(\mathbf{k},i\omega_n)e^{i\mathbf{k}\cdot\mathbf{r}}$ is the corresponding Fourier transform of the quasiparticle GF with a form factor of the localized electron. In the present continuum model, the positions of the nearest neighbor of the impurity $\mathbf{r}_0$ will be set according to our chosen parameters.

When the slave-boson mean field approximation is applied , the quasiparticle GF for the localized electron is derived as $\hat{G}_f(i\omega_n) = \left[i\omega_n - \tilde{\epsilon}_d\sigma_z - \hat{\Sigma}_f\left(i\omega_n\right)\right]^{-1}$, where the corresponding self-energy is given by

$$\hat{\Sigma}_f\left(i\omega_n\right) = \tilde{V}^2\sigma_z[\hat{G}_s^0(\mathbf{r}_0,i\omega_n) + \hat{G}^0\left(\mathbf{r}_0,i\omega_n\right)\hat{G}_p^0\left(i\omega_n\right)\hat{G}^0\left(\mathbf{r}_0,i\omega_n\right)]^{-1}\sigma_z, \tag{16}$$

where $\hat{G}_s^0(\mathbf{r}_0,i\omega_n) = \frac{1}{NV^2}\sum_{\mathbf{k}} V_{\mathbf{k}}^2\hat{G}_0(\mathbf{k},i\omega_n)$. In order to carry out further calculations, the various GFs introduced above are simplified as follows

$$\hat{G}_0(i\omega_n) = -i\omega_n\left(\frac{\pi N_F}{\Gamma}\right)\alpha(i\omega_n),$$

$$\hat{G}^0\left(\mathbf{r}_0, i\omega_n\right) = -\Delta_0\left(\frac{\pi N_F}{\Gamma}\right)\gamma(i\omega_n)\sigma_x,$$
$$\hat{G}_s^0(\mathbf{r}_0, i\omega_n) = -i\omega_n\left(\frac{\pi N_F}{\Gamma}\right)\gamma(i\omega_n), \tag{17}$$

with

$$\alpha(\omega) = \frac{2\Gamma}{\pi\Delta_0}\frac{1}{\sqrt{1+\left(\omega/\Delta_0\right)^2}}K\left(\frac{1}{\sqrt{1+\left(\omega/\Delta_0\right)^2}}\right); \tag{18}$$

$$\gamma(\omega) = \frac{2\Gamma}{\pi\Delta_0}\left[\sqrt{1+\left(\omega/\Delta_0\right)^2}E\left(\frac{1}{\sqrt{1+\left(\omega/\Delta_0\right)^2}}\right) - \frac{\left(\omega/\Delta_0\right)^2}{\sqrt{1+\left(\omega/\Delta_0\right)^2}}K\left(\frac{1}{\sqrt{1+\left(\omega/\Delta_0\right)^2}}\right)\right], \tag{19}$$

where $K(x)$ and $E(x)$ are the complete elliptical integrals of the first and second kind, respectively. At zero temperature, the ground-state energy changes due to the presence of Zn impurity and scalar potential are:

$$\delta\varepsilon = -\frac{1}{\pi}\int_0^D d\omega \ln\left(\omega^2\left[1+b_0^2\gamma(\omega)A_1(\omega)\right]^2 + \left[\tilde{\epsilon}_d - b_0^2A_2(\omega)\right]^2\right)$$
$$+\tilde{\epsilon}_d + \lambda_0\left(b_0^2-1\right),$$

where D is the band width of the normal conduction electrons, and

$$A_1(\omega) = 1 + \frac{\left(c\Delta_0\right)^2\alpha(\omega)\gamma(\omega)}{\Gamma^2 + c^2\omega^2\alpha^2(\omega)},$$
$$A_2(\omega) = \frac{-c\Gamma\Delta_0^2\ \gamma^2(\omega)}{\Gamma^2 + c^2\omega^2\alpha^2(\omega)}. \tag{20}$$

The saddle-point equations are thus derived as

$$\lambda_0 = \frac{1}{\pi}\int_0^D d\omega\frac{2\omega^2\gamma A_1(1+b_0^2\gamma A_1) - 2A_2(\tilde{\epsilon}_d - b_0^2A_2)}{\omega^2\left[1+b_0^2\gamma(\omega)A_1(\omega)\right]^2 + \left[\tilde{\epsilon}_d - b_0^2A_2(\omega)\right]^2}, \tag{21}$$

$$b_0^2 = \frac{1}{\pi}\int_0^D d\omega\frac{2\left(\tilde{\epsilon}_d - b_0^2A_2\right)}{\omega^2\left[1+b_0^2\gamma(\omega)A_1(\omega)\right]^2 + \left[\tilde{\epsilon}_d - b_0^2A_2(\omega)\right]^2}. \tag{22}$$

Notations here are the same as used in Eqs.(8) and (9). These equations are solved self-consistently to obtain the phase diagram which is essentially the same as for the Ni-doped case, *i.e.* the physics is dominated by the single-hole occupied state. Again, due to the presence of both attractive scalar potential and quantum impurity scatterings, localized resonant states in the quasiparticle spectrum are induced. However, unlike the Ni-doped

case, a dominant sharp resonance associated with the localized Anderson electron is formed above the Fermi level, while a small and broad resonance state associated with the scalar potential appears below the Fermi level. This difference is mainly due to the different location of the Anderson electron: on-site vs nearest neighbors. We plot the DOS for the localized electron $N_d(\omega)$ with different values of ϵ_d for two potential scattering strengths $c = 2$ and 5 in Fig.5. As ϵ_d moves up, the magnitude of the resonance above the Fermi level slightly decreases and the peak position is shifted away from the Fermi energy.

To compare with results for Ni substitution, the imaginary part of the retarded self-energy for the localized electron is calculated for the strengths of the potential scattering $c = 1, 2, 5$ and $\epsilon_d/\Delta_0 = -0.2$, displayed in Fig.6a. The main difference from the Ni doping case is that a single narrow resonance peak shows up below the Fermi level and becomes sharper as the strength of potential scattering is increasing. In Fig.6b, the spin relaxation function for the localized electron $S_d(\omega)$ is also shown. A magnetic oscillation is displayed and the amplitude is *one order of magnitude larger* than that in the Ni case (Please note the solid line corresponds to $c = 1$ now), implying the single $3d$ hole on the nearest neighbors of the Zn impurity atom does display a substantial local magnetic moment! [1,2] Certainly, we do not claim here a full explanation for the local magnetic moment formation induced by Zn impurity doping. However, our calculations do indicate the existence of a local magnetic moment on the nearest neighbors of the Zn impurity atom.

To confront the STM experimental results, we calculate the LDOS of the dSC quasiparticles around the Zn impurity sites under $\epsilon_d/\Delta_0 = -0.3, -0.1$ for two strengths of scalar potential $c = 2, 4$, displayed in Fig.7. The LDOS on the Zn impurity site has clearly shown that there are a very sharp resonance just below the Fermi level and a small and broad resonance above the Fermi level. The former is induced by the hybridization between the localized hole with the dSC quasiparticles, while the latter is caused by the potential scattering. Moreover, in contrast to the Ni substitution result, the DOS near the gap edges are completely suppressed to zero, which is consistent with the fact that the superconductivity may be suppressed by Zn impurities stronger than that by the Ni impurities. On the nearest

neighbor sites $\mathbf{r}_0 = (\pm a, 0)$ and $(0, \pm a)$, where $a = 0.05\xi$ and $\xi = \hbar v_F/\Delta_0$ is the coherence length of dSC state, two resonant peaks appear below and above the Fermi level, respectively. However, on the next nearest neighbor sites $\mathbf{r}_0 = \pm(a, a)$, the LDOS obtained is very much similar to that on the Zn impurity site. All these features are in good agreement with the STM experimental results [4].

Finally, the spatial distribution of the LDOS of the dSC quasiparticles is calculated. The LDOS around the Zn impurity at the main resonance energy is displayed in Fig.8a for the hole-like excitations $\omega = -\Omega_{res}$ and in Fig.8b for $\omega = \Omega_{res}$ for the electron-like excitations as a function of spatial variables for $c = 1, 2$, and 3 with $\epsilon_d/\Delta_0 = -0.05$ in a logarithmic intensity scale. The quasiparticle resonances induced by the doped non-magnetic impurity are extended from the impurity to one coherence length of dSC. The largest amplitude of the quasiparticle resonance occurs at the neighborhood of the impurity, particularly at the next nearest neighbors, and the local electronic structures at distances $r \ll \xi$ drastically differ in Fig.8a from Fig.8b. However, further away from the impurity site, both structures of the LDOS are almost the same, where the enhanced LDOS is extended along the gap maxima directions. Moreover, the spatial LDOS of the dSC quasiparticles is not enhanced as the strength of the scalar potential is increasing. The LDOS pattern in the left column for $c = 1$ case is closer to the distribution of LDOS obtained from the STM spectra [4]. These results seem to show that the strength of potential scattering in the present model Hamiltonian, needed to describe the experimental data is not as strong as assumed in previous studies with purely potential scattering [6,8].

IV. CONCLUSIONS

In this paper, we propose an effective model Hamiltonian of an Anderson localized electron (hole) hybridizing with $d_{x^2-y^2}$-wave BCS type superconducting quasiparticles supplemented with an attractive scalar potential at the impurity site. Within a unified framework, we can describe the non-magnetic (Zn) and magnetic (Ni) impurity scatterings for cuprate

superconducting quasiparticles of optimally doped high T_c materials.

Due to the nature of d-wave superconducting quasiparticles, both quantum scattering on localized electron and scalar potential scatterings are relevant interactions in the low energy limit, showing a strong interplay with each other and leading to localized resonant states below the maximal superconducting gap. In the Ni case, two localized resonant states are formed above the Fermi level in the LDOS at the doped impurity site, while in the Zn case a sharp resonant peak caused by the localized hole is found just below the Fermi level to dominate the LDOS at the Zn impurity site, accompanied by a small and broad bound state above the Fermi level induced by the potential scattering. These characteristic features are in exact agreement with experiments [4,5]. Moreover, the spatial patterns of the resonant states in Zn and Ni doped cases are quite different in STM experiments. It is significant that these differences can be reproduced easily in our simple model. *The key assumption is that the* $3d$ *electron is located on the Ni site, while it is distributed over nearest neighbor Cu ions in the Zn-doped case due to the local antiferromagnetic background.* The excellent agreement with experiments convincingly demonstrates the correctness of this assumption and the self-consistency of our model. We would emphasize these are generic features of our model, not due to adjustable parameters in the theory to fit the experiments.

We should point out that in both cases, there are no Kondo screening effects on the local magnetic moment due to the localized electrons, *i.e.*, the local magnetic moments do not couple to the superconducting quasiparticles in the low energy limit, and the dominant behavior is the single hole occupied state, characterized by a strong hybridization between the localized and delocalized electrons. Moreover, from the calculations of the spin relaxation functions for the localized electron in both Ni and Zn doped materials, we find that the additional $3d$ localized hole displays a weak magnetic oscillation. Such a magnetic behavior is consistent with the spin-1/2 magnetic moment observed in NMR measurements.

We would like to mention that our results do not contradict those of the Kondo model study for systems with reduced density of states at the Fermi level [11–13,15,26,27] or d-wave superconductors. The important factor in those studies is the presence of a strong

particle-hole asymmetry, due to, for example, the potential scattering. The behavior of systems controlled by the "strong asymmetric coupling" fixed point is very similar to what we have obtained here. In particular, there is no single Kondo resonance peak at the Fermi level in that case, either. Instead, the resonance is shifted from the Fermi level by the energy of the order T_K. In our opinion, identifying this resonance peak to the standard Kondo screening effect is somewhat misleading. The NMR experiments in Ni, Zn-doped cuprates samples [1,2,28] can be interpreted using the "Kondo temperature" T_K as a characteristic energy scale. Recent experiment [28] seems to show such a scale exists even in the superconducting state. On the contrary, the SQUID measurements do not exhibit any signature of such a "Kondo" scale. [3] We believe the resistivity measurements would be able to identify contributions from the Kondo scattering. However, our paper and related studies [11–13,15,26,27] demonstrate that in low temperature superconducting state one should not expect the standard Fermi liquid behavior, corresponding to the Kondo strong-coupling limit. To our feeling, the effective Anderson model used in our paper has the advantage of treating different physical situations in a unified self-consistent fashion.

A few related remarks are in order:

(1) In this paper we did not address the issue of the magnetic moment formation in non-magnetic doping case. A lot of efforts have been devoted to this problem [29], but it is still not fully understood, in particular, the issue of spinon confinement which is the key argument for the "proof", is entirely open. What we have been doing is to assume the existence of the local moment, described by the Anderson model and find out that the final results are consistent with the starting assumption.

(2) To reconcile the discrepancy of the potential scattering model [6] with the STM experiments on Zn-doped BSCO, namely, the presence of a strong resonance peak at the Zn site in experiments, the argument of tunneling matrix element between layers (so-called "filter" effect) [7,30] was suggested. We have not included this effect in our calculations to confront the STM experiments. To our knowledge, this issue is still open, and the Kondo model calculation [11,13] seems to show the same — irrelevance of this effect.

(3) We have not considered the effect of disorder on the quasiparticle density of states in dSC which may not vanish at the Fermi level. This is still an issue under debate. [31] Our hope is that the main conclusions of our paper will survive in the limit of dilute doping. The case of strong disorder is beyond the scope of our present work.

(4)The interplay of magnetic and non-magnetic scatterings is always important for superconducting states even in the s-wave case [25]. It is true that the potential scattering alone cannot give rise to a bound state inside the gap in that case (Anderson theorem). However, the presence of the potential scattering will affect the position of the bound state due to the magnetic moment scattering (see first paper of Ref. [25]). What we have shown is that the scattering behavior in the d-wave nodal direction is quite different from the s-wave superconductor, whereas in the gap maximum direction it is rather similar. For the low-energy physics, the quantum magnetic scattering is the dominant effect. Finally, we would emphasize once again that our result is valid only in the strong coupling, large U-limit of the Anderson impurity in a d-wave superconductor, which is very different from that for the conventional normal metallic state.

Acknowledgments

We would like to thank K. Ingersent, S. H. Pan, M. Vojta and T. Xiang for useful discussions. One of the authors (G.-M. Zhang) would like to thank the hospitality of Abdus Salam International Center for Theoretical Physics, where part of this work is completed, and acknowledges the financial support from NSF-China (Grant No. 10074036 and 10125418) and the Special Fund for Major State Basic Research Projects of China (G2000067107).

REFERENCES

[1] J. Bobroff, W. A. MacFarlane, H. Alloul, P. Mendels, N. Blanchard, G. Collin, and J.-F. Marucco, Phys. Rev. Lett. **83**, 4381 (1999); A.V. Mahajan, H. Alloul, G. Collin, and J.F. Marucco, Eur. Phys. J. B **13**, 457 (1999).

[2] M.-H. Julien, T. Fehér, M. Horvatić, C. Berthier, O. N. Bakharev, P. Ségransan, G. Collin, and J.-F. Marucco , Phys. Rev. Lett. **84**, 3422 (2000).

[3] P. Mendels, J. Bobroff, G. Collin, H. Alloul, M. Gabay, J. F. Marucco, N. Blanchard and B. Grenier, Physica C **235-240**, 1595 (1994); *ibid*, Europhys. Lett. **46**, 678 (1999).

[4] E. W. Hudson, S. H. Pan, A. K. Gupta, K.-W. Ng, and J. C. Davis, Science **285**, 88 (1999); A. Yazdani, C. M. Howald, C. P. Lutz, A. Kapitulnik, and D. M. Eigler, Phys. Rev. Lett. **83**, 1761 (1999); S. H. Pan, E. W. Hudson, K. M. Lang, H. Eisaki, S. Uchida, and J. C. Davis, Nature (London) **403**, 746 (2000).

[5] E. W. Hudson, K. M. Lang, V. Madhavan, S. H. Pan, H. Eisaki, S. Uchida, and J. C. Davis, Nature (London) **411**, 920 (2001).

[6] A. V. Balatsky, M. I Salkola, and A. Rosengren, Phys. Rev. B **51**, 15547 (1995); M. A. Salkola, A. V. Balatsky, and D. J. Scalapino, Phys. Rev. Lett. **77**, 1841 (1996); M. I. Salkola, A. V. Balatsky, and J. R. Schrieffer, Phys. Rev. B **55**, 12648(1997).

[7] I. Martin, A. V. Balatsky, and J. Zaanen, Phys. Rev. Lett. **88**, 097003 (2002).

[8] M. E. Flatté and J. M. Byers, Phys. Rev. Lett. **80**, 4546 (1998); M. E. Flatté, Phys. Rev. B **61**, R14920 (2000).

[9] H. Tsuchiura, Y. Tanaka, M. Ogata and S. Kashiwaya, J. Phys. Soc. Jpn, **68**, 2510 (1999); *ibid*, Phys. Rev. Lett. **84**, 3165 (2000).

[10] S. Haas and K. Maki, Phys. Rev. Lett. **85**, 2172 (2000).

[11] A. Polkovnikov, S. Sachdev, and M. Vojta, Phys. Rev. Lett. **86**, 296 (2001); A.

Polkovnikov, Phys. Rev. B **65**, 064503 (2002).

[12] J. -X. Zhu and C. S. Ting, Phys. Rev. B **63**, R020506 (2001); *ibid*, Phys. Rev. B **64**, R060501 (2001).

[13] M. Vojta and R. Bulla, Phys. Rev. B **65**, 014511 (2002).

[14] D. Withoff and E. Fradkin, Phys. Rev. Lett. **64**, 1835 (1990); C. R. Cassanello and E. Fradkin, Phys. Rev. B **56**, 11246 (1997).

[15] K. Ingersent, Phys. Rev. B **54**, 11936 (1996); C. Gonzalez-Buxton and K. Ingersent, *ibid*. **57**, 14254 (1998), and references therein.

[16] G. -M. Zhang, H. Hu and L. Yu, Phys. Rev. Lett. **86**, 704 (2001).

[17] Y. Sidis, P. Bourges, H. F. Fong, B. Keimer, L. P. Regnault, J. Bossy, A. Ivanov, B. Hennion, P. Gautier-Picard, G. Collin, D. L. Millius, and I. A. Aksay, Phys. Rev. Lett. **84**, 5900 (2000).

[18] R. Gupta and M. Gupta, Phys. Rev. B **59**, 3381 (1999).

[19] T. Xiang, Y.H. Su, C. Panagopoulos, Z.B. Su, and L. Yu, cond-mat/0205607.

[20] S. E. Barnes, J. Phys. F. **6**, 1375 (1976).

[21] P. Coleman, Phys. Rev. B **29**, 3035 (1984).

[22] P. Coleman, Phys. Rev. B **35**, 5072 (1987).

[23] C. M. Varma, P. B. Littlewood, S. Schmitt-Rink, E. Abrahams and A. E. Ruckenstein, Phys. Rev. Lett. **63**, 1996 (1989).

[24] T. A. Costi and C. Kieffer, Phys. Rev. Lett. **76**, 1683 (1996); T. A. Costi, *ibid.*, **80**, 1038 (1998).

[25] Lu Yu, Acta Physica Sinica **21**, 75 (1965); H. Shiba, Progr. Theor. Phys. **40**, 435 (1968).

[26] S. Fujimoto, Phys. Rev. B **63**, 024406 (2000).

[27] M. Vojta, cond-mat/0102089.

[28] J. Bobroff, H. Alloul, W. A. MacFarlane, P. Mendels, N. Blanchard, G. Collin, and J.-F. Marucco, Phys. Rev. Lett. **86**, 4116 (2001).

[29] See. *e.g.*, A. M. Finkelstein, V. E. Kataev, E. F. Kukovitskii, and G. B. Teitelbaum, Physica C **168**, 370 (1990); G. Khaliullin, R. Kilian, S. Krivenko, and P. Fulde, Phys. Rev. B **56**, 11882 (1997); R. Kilian, S. Krivenko, G. Khaliullin, and P. Fulde, Phys. Rev. B **59**, 14432 (1999).

[30] J. -X. Zhu, C. S. Ting, C. R. Hu, Phys. Rev. B **62**, 6207 (2000).

[31] See, *e.g.* A. A. Nersesyan, A. M. Tsvelik, and F. Wegner, Phys. Rev. Lett. **72**, 2628 (1994); W. A. Atkinson, P. J. Hirschfeld, A. H. MacDonald, and K. Ziegler, Phys. Rev. Lett. **85**, 3926 (2000) and references therein; A. M. Martin, G. Litak, B. L. Gyorffy, J. F. Annett, K. I. Wysokinski, Phys. Rev. B **60**, 7523 (1999).

Figures Captions

Fig. 1. The DOS $N_d(\omega)$ of the localized electron, (a) for $c = 1$ and (b) for $c = 2$, with $\epsilon_d/\Delta_0 = -0.05$, 0.05, 0.15, and 0.30, denoted by solid, dashed, dotted, and dash-dotted lines, respectively.

Fig. 2. The imaginary part of the self-energy for the localized electron is delineated in (a), and the corresponding local spin relaxation function $S_d(\omega)$ in (b), for $\epsilon_d/\Delta_0 = -0.05$ and for $c = 0$, 1 and 2, represented by solid, dashed, and dash-dotted lines, respectively..

Fig. 3. The LDOS $N_c(r{=}0.07\xi, \omega)$ of the dSC quasiparticles for different potential scattering strengths $c = 2$ and 5, with $\epsilon_d/\Delta_0 = 0.0$ (solid line), and 0.3 (dashed lines) in units of N_F. (a) and (c) are along the directions of the gap maxima, while (b) and (d) along the directions of the gap nodes.

Fig. 4. The spatial distributions of the conduction electron LDOS around the Ni impurity at the first resonant energy for $c = 1, 2$ and 3. (a) $\omega = -\Omega^1_{res}$ and (b) $\omega = +\Omega^1_{res}$. Here $\epsilon_d/\Delta_0 = -0.05$, and a logarithmic intensity scale is used. The ranges of x and y in each subplot are set from -0.6ξ to $+0.6\xi$, and ξ is the coherence length.

Fig. 5. The DOS of the localized electron $N_d(\omega)$. (a) corresponds to $c = 2$, and (b) to $c = 5$, with $\epsilon_d/\Delta_0 = -0.4$, -0.2, and 0.0, denoted by solid, dashed, and dash-dotted lines, respectively.

Fig. 6. The imaginary part of the self-energy for the localized electron is displayed in (a), and the corresponding spin relaxation function $S_d(\omega)$ in (b) for $\epsilon_d/\Delta_0 = -0.2$ and for $c = 1, 2$ and 5, denoted by solid, dashed, and dash-dotted lines, respectively.

Fig. 7. The LDOS of the dSC quasiparticles on the Zn impurity site, on the nearest neighbor sites, and on the next nearest neighbor sites with $\epsilon_d/\Delta_0 = -0.3$ (solid line), and -0.1 (dashed lines) in units of N_F. (a) corresponds to $c = 2$, and (b) to $c = 4$.

Fig. 8. The spatial distributions of the LDOS of dSC quasiparticles around the Zn impurity at the resonant energy for $c = 1, 2$ and 3. (a) $\omega = -\Omega_{res}$ and (b) $\omega = +\Omega_{res}$. Here $\epsilon_d/\Delta_0 = -0.2$ and a logarithmic intensity scale is used. The ranges of x and y in each

subplot are set from -0.3 to $+0.3$ in units of the coherent length ξ.

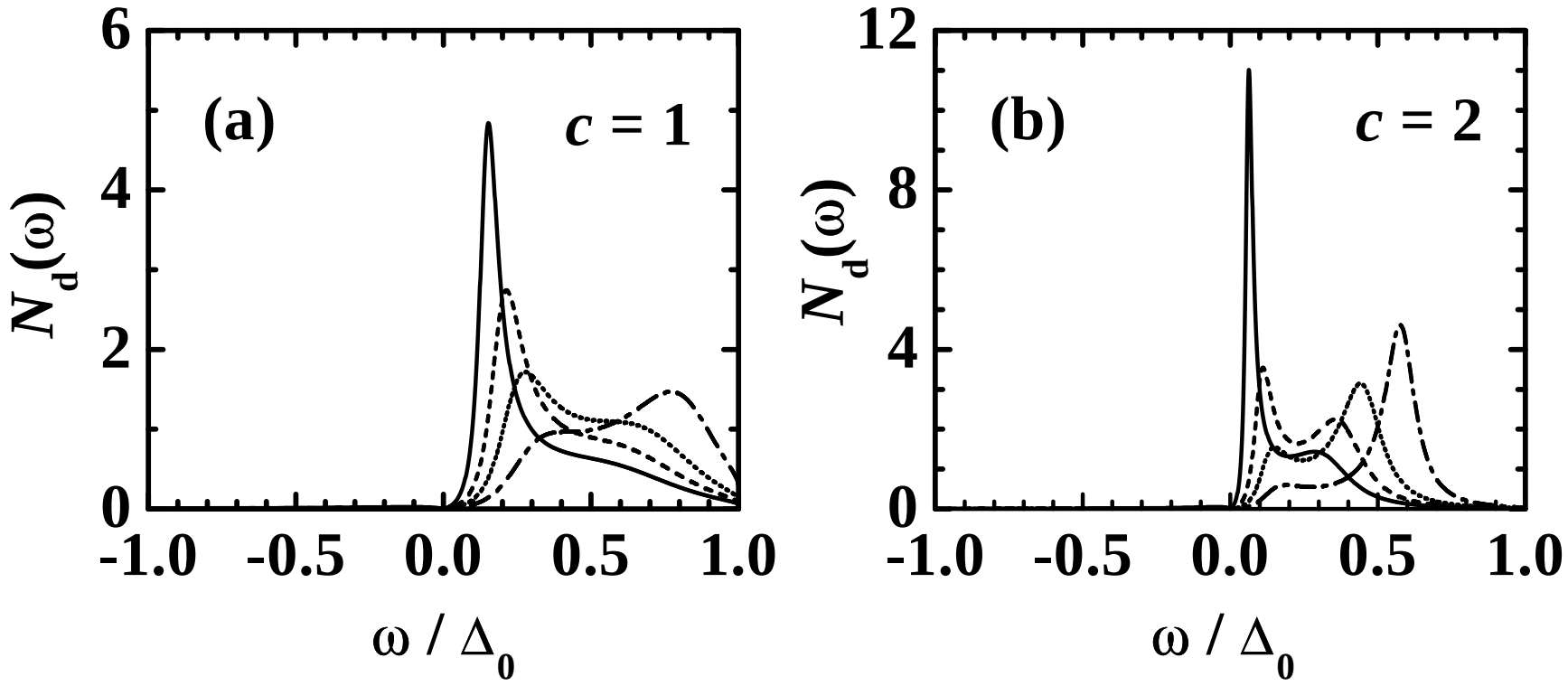

Fig.1 G. M. Zhang *et al.*

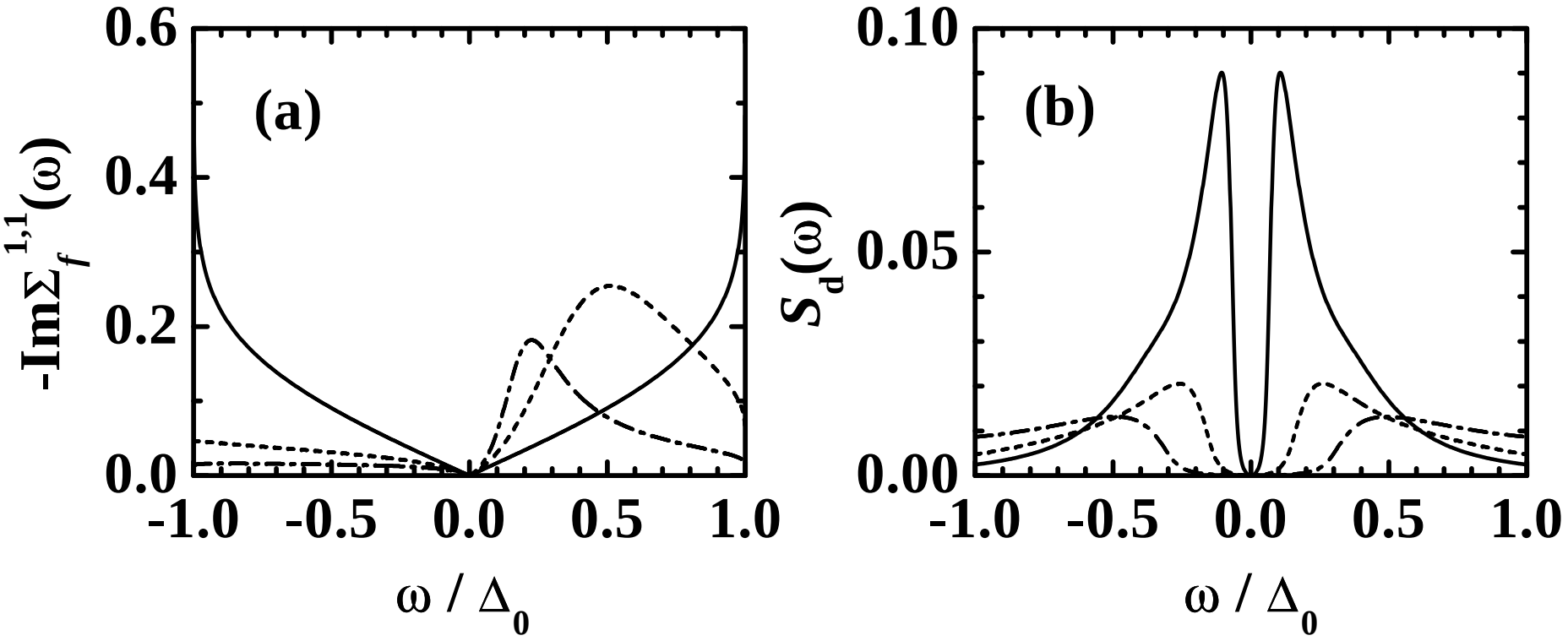

Fig.2 G. M. Zhang *et al.*

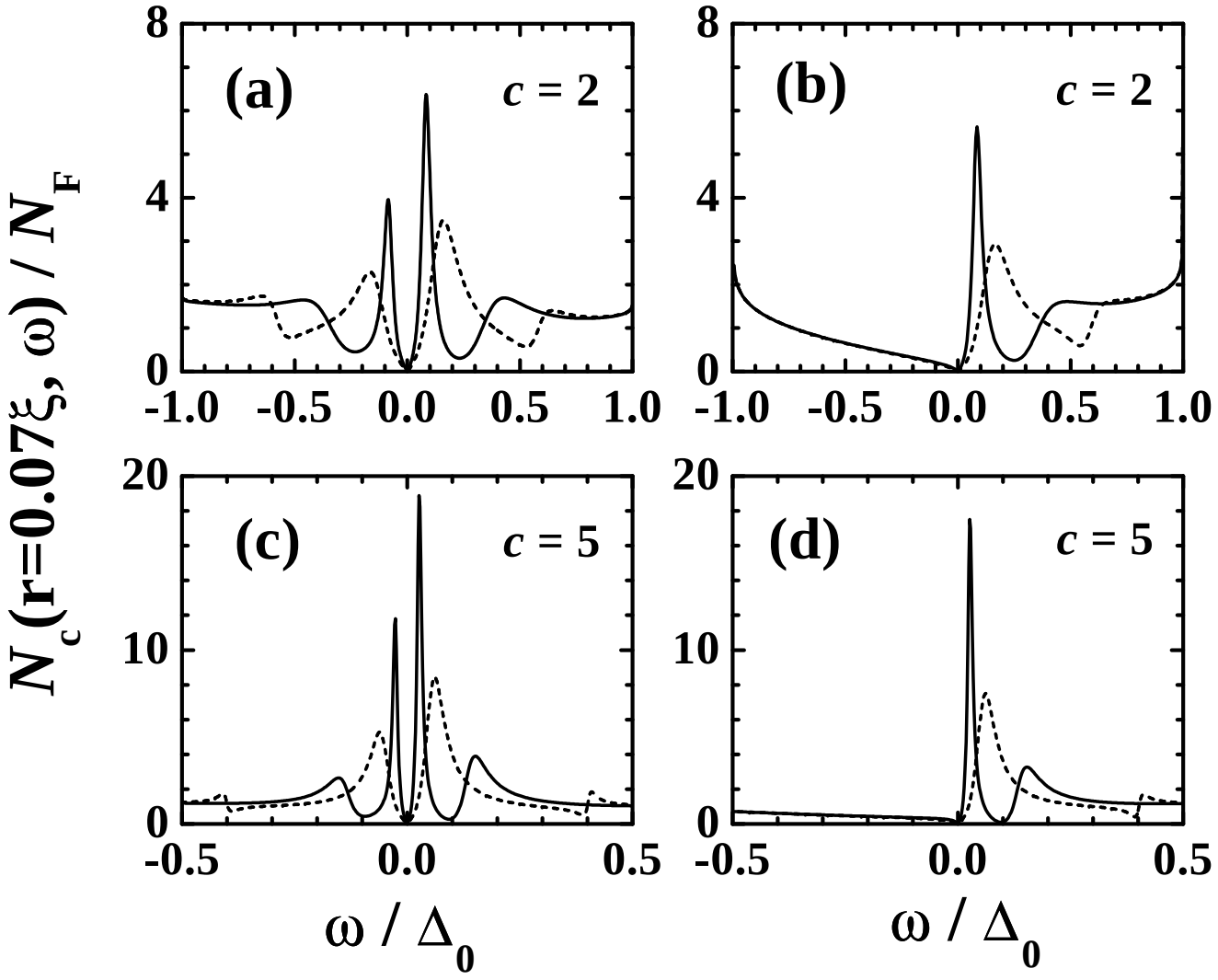

Fig.3 G. M. Zhang *et al.*


This figure "zhy0528_fig4.jpg" is available in "jpg" format from:
http://arXiv.org/ps/cond-mat/0206133v1

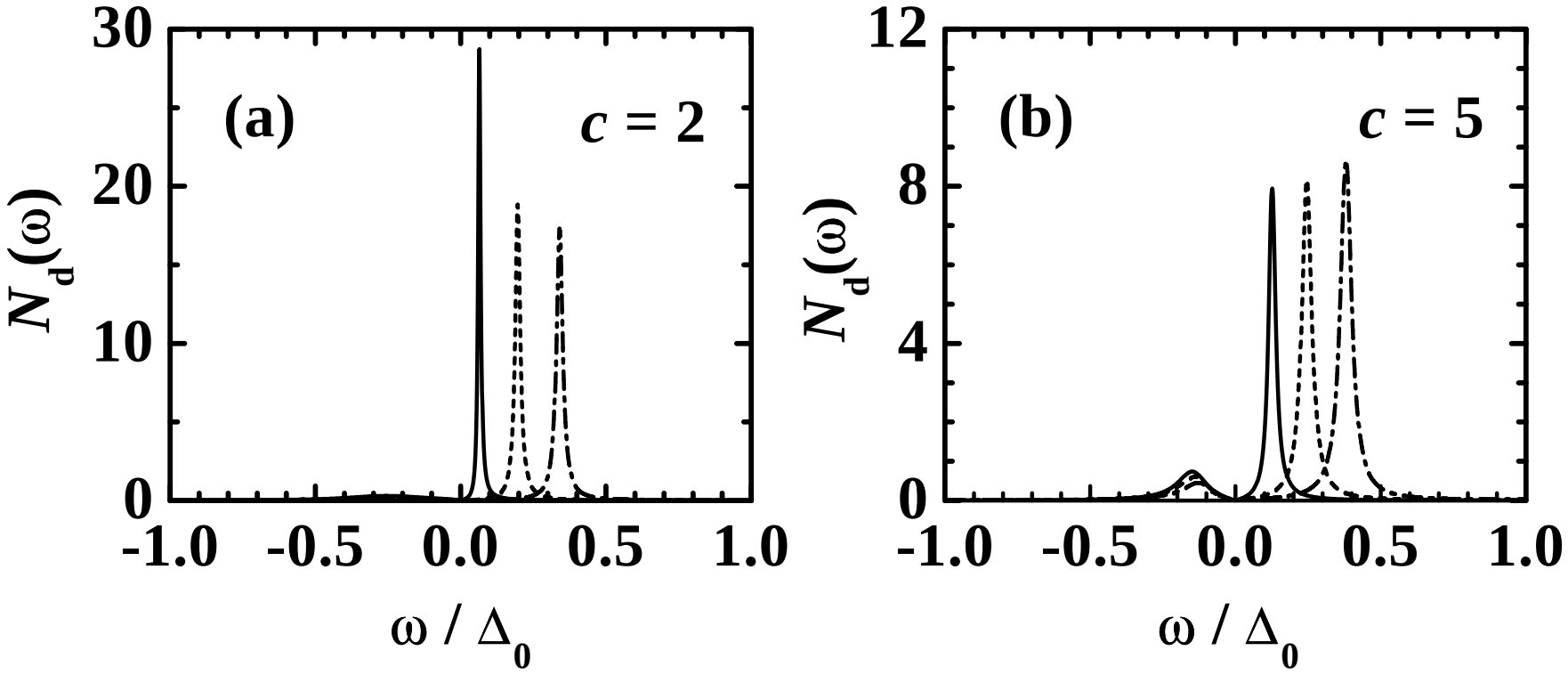

Fig.5 G. M. Zhang *et al.*

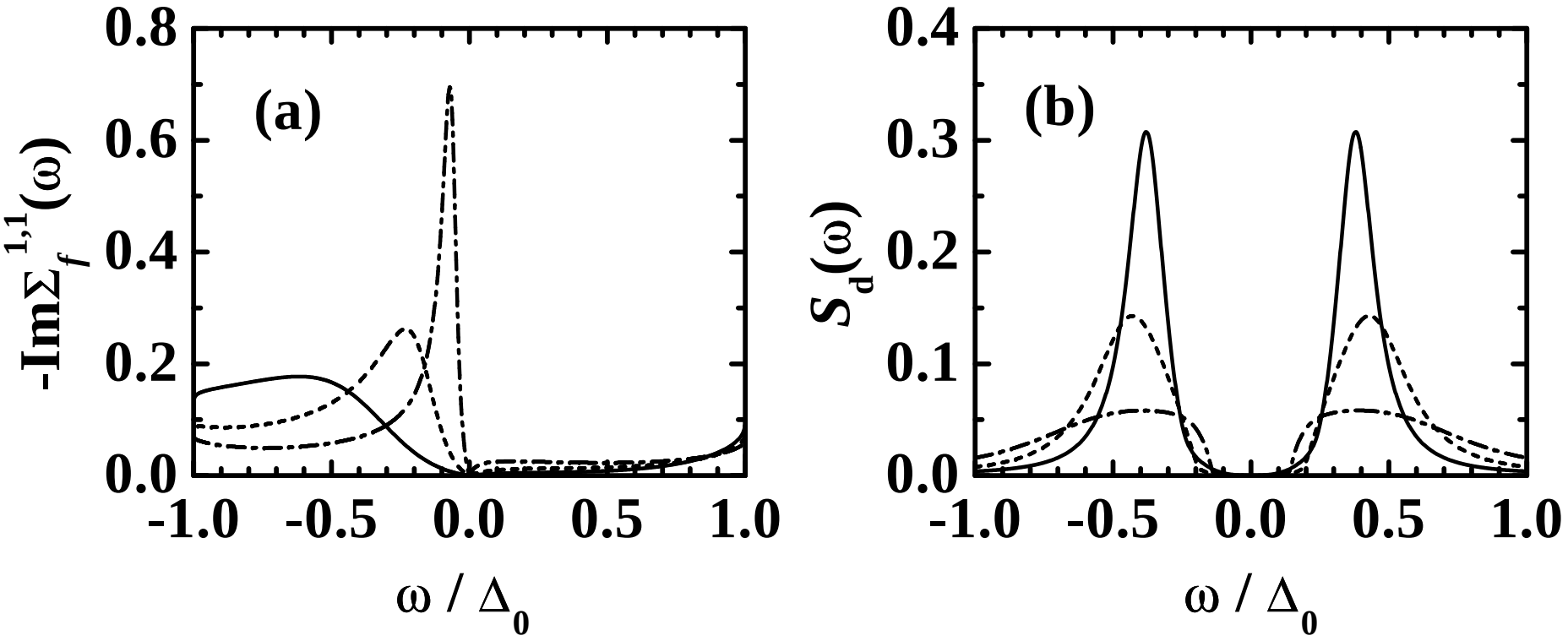

Fig.6 G. M. Zhang *et al.*

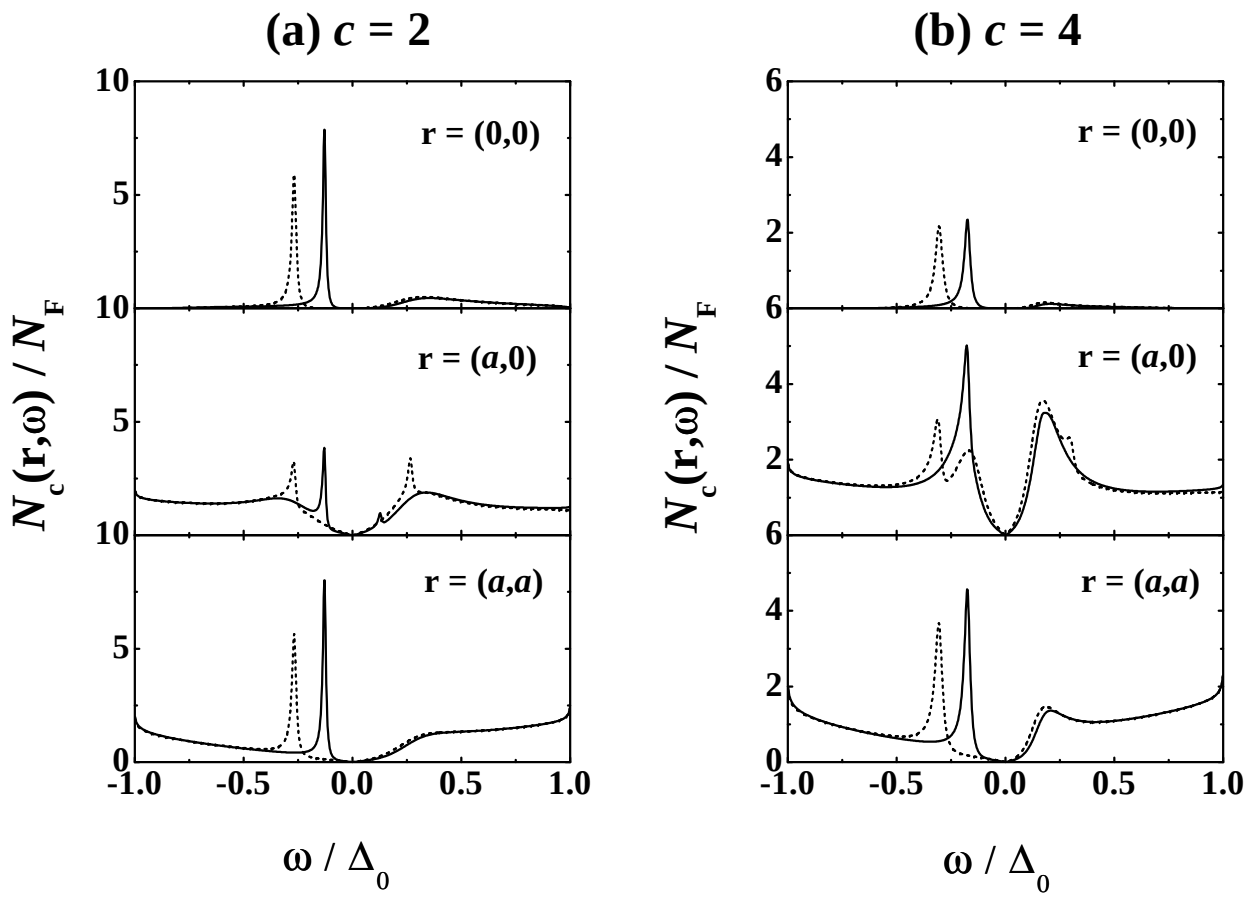

Fig.7 G. M. Zhang *et al.*


This figure "zhy0528_fig8.jpg" is available in "jpg" format from:
http://arXiv.org/ps/cond-mat/0206133v1